

## **Supporting Information**

### **Efficient Utilizing the Active Sites of MXene: MXene/PSSNa Films with 3D-Stabilized Porous Structure as High-Capacitance and High-Rate Electrodes for Flexible Supercapacitors**

Ying Song, Yaqing Liu, Qi Ao, Lin Jiang, Xiaoxiao Lv, Xinglai Tong, Tuohao Jiang,  
Yuanqing Yao, Jun Tang\*

## Materials and methods

### Chemicals

Ti<sub>3</sub>AlC<sub>2</sub> was obtained from 11 Technology Co. LTD., hydrochloric acid (HCl) was obtained from Chinese Medicine Reagent Co. LTD. Energy chemical supplied the Sodium 4-vinylbenzenesulfonate (SSNa), 2-bromo-2-methylpropionyl bromide (BiBB), N, N, N', N', N''-pentamethyldiethylenetriamine (PMDETA), Potassium hydroxide (KOH), Copper (II) bromide (CuBr<sub>2</sub>), Sodium L-ascorbate (L-ASC), Lithium fluoride (LiF) and Triethylamine (TEA). Every reagent used in this research was of analytical quality and had not been subjected to additional purification. Every water-based solution was formulated with deionized water (exceeding 18 MΩ).

### Preparation of MXene (Ti<sub>3</sub>C<sub>2</sub>T<sub>x</sub>) with few layers

Added 1 g of LiF and 20 mL of 9 M hydrochloric acid solution into a 50 mL PTFE beaker and stir them in an ice water environment for 30 min to dissolve LiF fully. Then, slowly added 1 g of Ti<sub>3</sub>AlC<sub>2</sub> to the beaker and seal the beaker and raised temperature to 35 °C for 24 h (400 rpm). After that, the obtained black liquid was centrifuged (3500 rpm, 10 min), the lower sediment was collected and the pH of the upper clear liquid was washed repeatedly with deionized water. The final black precipitate was dispersed with deionized water, ultrasonic for 1 h, centrifugation (3500 rpm, 1 h), and the upper layer of dark green liquid was collected, which was a small layer of Ti<sub>3</sub>C<sub>2</sub>T<sub>x</sub> dispersion. Finally, the black powder solid, MXene was obtained by freeze-drying of a few layers of Ti<sub>3</sub>C<sub>2</sub>T<sub>x</sub> dispersion, and it was stored in a low temperature and dry environment.

### Preparation of MOH

400 mg MXene powder was dispersed in KOH solution (50 mL, 2 M) and stirred

continuously for 12 h (800 rpm, nitrogen atmosphere) in an ice bath, centrifuged (7000 rpm) after the reaction was complete. The black sediment was gathered and underwent multiple washes with deionized water until it reached a pH below 8 in the clear upper solution. The produced black sediment underwent freeze-drying to achieve, MXene with polyhydroxy-modified surface (MOH).

## Preparation of MBr

200 mg of MOH and 0.53 mL of TEA were dispersed into 20 mL of DMF, and then BiBB dissolved in 5 mL of DMF was slowly added to the mixture of MOH/TEA/DMF under 0 °C nitrogen atmosphere. After reaction for 24 h, centrifuged (7000 rpm) and washed the lower precipitate 4-5 times with deionized water, and the product MBr was obtained by freeze-drying.

## Preparation of MPS

100 mg of MBr, 100 mg of SSNa, 21.5 mg of CuBr<sub>2</sub>, 50 μL of PMEDTA were dispersed into 5 mL of deionization and placed in the oil bath at 30 °C after nitrogen purge for 30 min. 28.7 mg of L-ASC was added to the mixture under nitrogen atmosphere, stored at 30 °C for 1 h, and heated at 60 °C for 24 h, then the system was cooled to room temperature and exposed to air to stop the reaction. The resulting product was washed several times in deionized water and freeze-dried to obtain a black powder solid, which was represented as MPS. At the same time, as a control, the mass of MBr was changed to 20 mg, 60 mg, 140 mg, 180 mg, and the corresponding SSNa mass was 180 mg, 140 mg, 60 mg, 20 mg. The above operations were repeated, and the products obtained were recorded as MPS-1 and MPS-2, MPS-4, MPS-5, respectively.

## Preparation of MPS/ carbon cloth (CC) electrodes

Mixed MPS, graphite and CMC according to the mass ratio of 80:10:10 and grind

evenly. Brush the ground mixture onto the cleaned carbon cloth. The MPS/CC electrode was obtained by placing the carbon in a vacuum drying oven at 40 °C for 6 h. Electrode materials with different mass loads can be obtained by changing the mass of the mixture. The obtained film with a mass load of 4 mg cm<sup>-2</sup> was cut into 104 cm strips and stretched at a speed of 5 mm min<sup>-1</sup>.

### Preparation of Ti<sub>3</sub>C<sub>2</sub>T<sub>x</sub>@MPS electrodes

MPS and MXene were dispersed into deionized water in different proportions named Ti<sub>3</sub>C<sub>2</sub>T<sub>x</sub>@MPS-x (x was the mass fraction of MPS), and films with different mass loads were produced through vacuum filtration.

### Preparation of PVA/H<sub>2</sub>SO<sub>4</sub> gel electrolyte and symmetrical flexible supercapacitor

Added 1 g of PVA into 10 mL of deionized water, and stirred in an oil bath at 85 °C (500 rpm) for 6 h, achieving a clear and transparent PVA solution. Then 0.54 mL concentrated sulfuric acid was slowly added to the vigorously stirred PVA solution and continued to heat for 6 h to obtain a yellowish viscous PVA/H<sub>2</sub>SO<sub>4</sub> liquid. After cooling to room temperature, it was evenly coated on the surface of Ti<sub>3</sub>C<sub>2</sub>T<sub>x</sub>@MPS electrode with a brush, dried at room temperature overnight, and another piece of Ti<sub>3</sub>C<sub>2</sub>T<sub>x</sub>@MPS electrode was covered on its surface to obtain a symmetrical flexible supercapacitor with sandwich structure.

### Characterization

The morphology of various materials was observed using JEOL JSM-6700F field-emission scanning electron microscope (SEM), atomic force microscopy (AFM, Bruker Icon-XR) and transmission electron microscopy (JEM-2100F). Energy dispersive X-ray spectroscopy (EDX) was performed on an electron microscope at an accelerating

voltage of 20 kV. measurements conducted on the Nova nano 450 instrument. X-ray diffraction (XRD) analysis of the samples was collected on a PANalytical B.V. Empyrean. X-ray photoelectron spectroscopy (XPS) analysis of the samples was collected on a Thermo Fisher ESCALAB 250Xi. Fourier transform infrared (FT-IR) analysis of the samples was collected on a Shimadzu FT-IR 8400S. Thermogravimetric analysis (TGA, TA Q500) was performed from 30 °C to 800 °C at a heating rate of 10 °C min<sup>-1</sup> in N<sub>2</sub> flow. Brunauer-Emmett-Teller (BET) specific surface area and the mean porous equivalent diameters were determined by using a porosimeter (Micromeritics ASAP 2020, United States). Raman spectra was measured on LabRAM HR Evolution high resolution Raman spectrometer (scanning range: 100~800 cm<sup>-1</sup>, excitation wavelength: 514 nm). CHI660C electrochemical workstation was used to explore relevant electrochemical properties.

## Electrochemical testing of materials

The electrochemical properties of electrode materials were measured at room temperature using a three-electrode system. The prepared MPS/CC electrodes and Ti<sub>3</sub>C<sub>2</sub>T<sub>x</sub>@MPS electrodes were used as the working electrodes (using glass carbon electrode clamp), Ag/AgCl (saturated KCl) as the reference electrode, activated carbon as the counter electrode, and 3 M H<sub>2</sub>SO<sub>4</sub> as the electrolyte solution. Galvanostatic charge discharge (GCD) and cyclic voltammetry (CV) were performed at room temperature by using an electrochemical workstation. electrochemical impedance spectroscopy (EIS) and other tests. EIS had a test range of 0.1 to 100,000 Hz with a voltage amplitude of 5 mV. The cyclic stability of electrodes and flexible symmetric supercapacitors is tested at room temperature using a battery test system.

Prior to the test, MPS/CC and Ti<sub>3</sub>C<sub>2</sub>T<sub>x</sub>@MPS electrodes were activated with CV in 3 M H<sub>2</sub>SO<sub>4</sub> electrolyte (sweep speed of 10 mV s<sup>-1</sup>, voltage window of -0.6~0.2 V

(vs. Ag/AgCl), 120 cycles).

A comprehensive scan was conducted at a rate of 0.001V/s across a wide spectrum of voltage windows. Upon observing a distinct REDOX peak in the curve, manual reverse scanning was performed accordingly. Ultimately, based on these experimental findings, the optimal voltage window was determined to be -0.6-0.2V.

## DFT calculation

We use Materials Studio software to perform relevant DFT calculations.

The Forcite module was used for model optimization and numerical calculation of binding energy calculation.

The dmol3 module was used for model optimization and numerical calculation of band energy and DOS calculation. To lower the computational cost, we reduced the a and b dimensions and randomly chose two short chains of polymers to attach to two -OH on MXene. For all of the structural optimizations, the electronic convergence threshold was set to  $10^{-6}$  eV, the force was converged to  $0.002 \text{ Ha } \text{\AA}^{-1}$ , the maximum step size of each optimized atom move is  $0.3 \text{ \AA}$  and sampled the Brillouin zone with a k-spacing of fine.

## XAFS data

The obtained XAFS data was processed in Athena (version 0.9.26)[1] for background, pre-edge line and post-edge line calibrations. Then Fourier transformed fitting was carried out in Artemis (version 0.9.26) [2]. The  $k^3$  weighting, k-range of 3 –  $\sim 12 \text{ \AA}^{-1}$  and R range of 1 - 3  $\text{\AA}$  were used for the fitting of Ti-foil; The  $k^3$  weighting, k-range of 3 –  $\sim 9.0 \text{ \AA}^{-1}$  and R range of 1 - 3  $\text{\AA}$  were used for the fitting of Samples.

For Wavelet Transform analysis, the  $\chi(k)$  exported from Athena was imported into the Hama Fortran code. The parameters were listed as follow: R range, 0 - 4  $\text{\AA}$ ; k range,

0 – 16 Å<sup>-1</sup>; k weight, 2; and Morlet function with  $\kappa=10$ ,  $\sigma=1$  was used as the mother wavelet to provide the overall distribution.

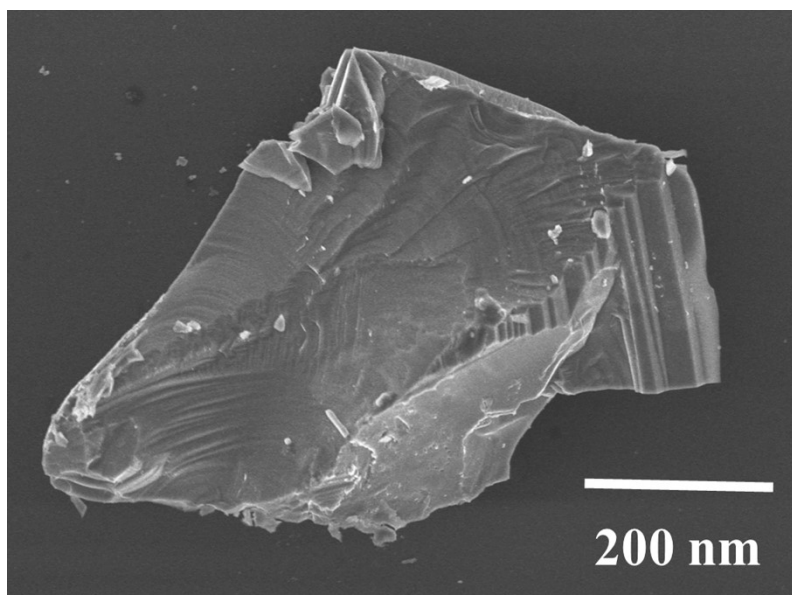


**Figure S1.** SEM of (A) MAX, (B) multilayered MXene

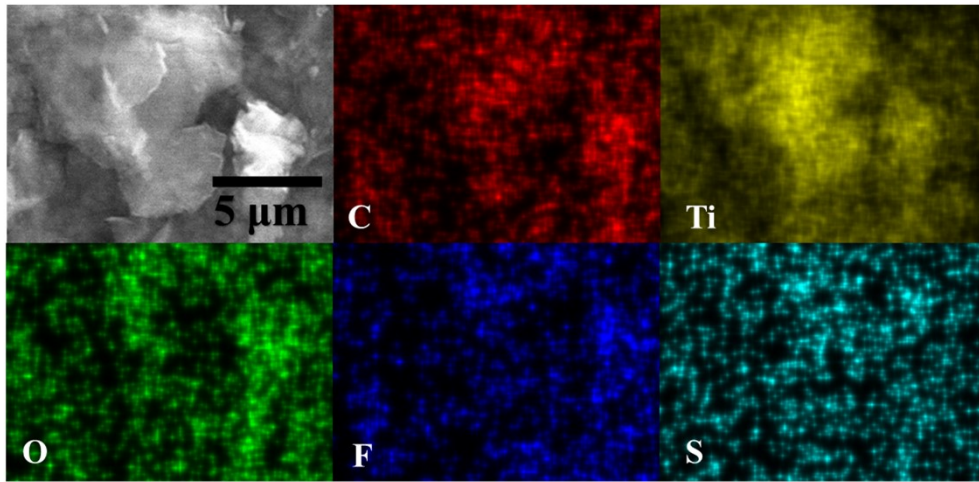


**Figure S2. Images of EDX elemental mapping of C, O, Ti, F, S for MPS**

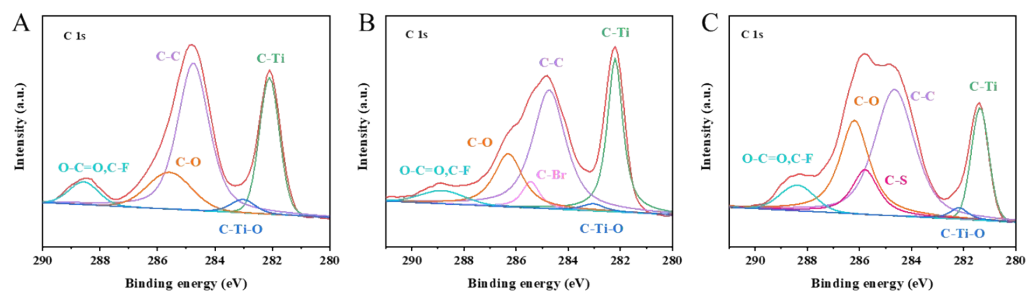


**Figure S3.** C 1s core-level XPS spectra of (A) MOH, (B) MBr and (C) MPS.

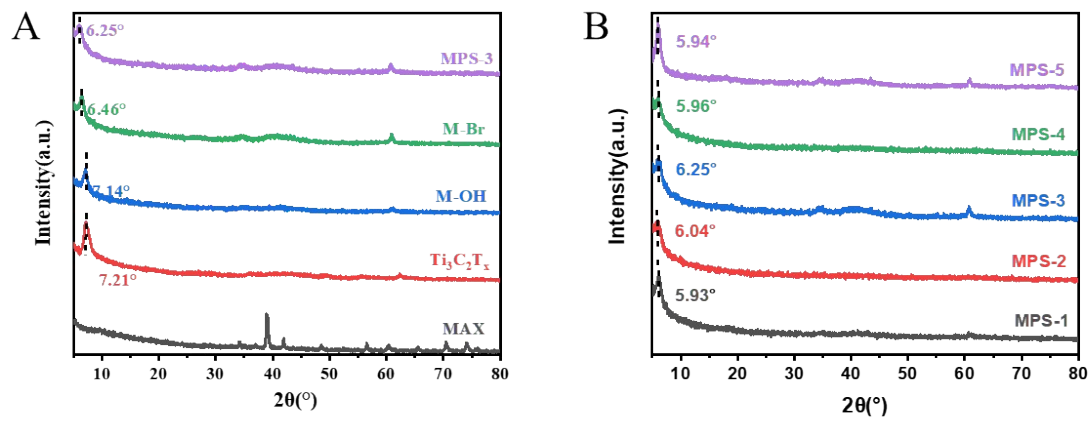


**Figure S4.** XRD patterns of (A) the MAX,  $Ti_3C_2T_x$ , MOH, MBr and MPS-3 powder, (B) MPS-1~MPS-5

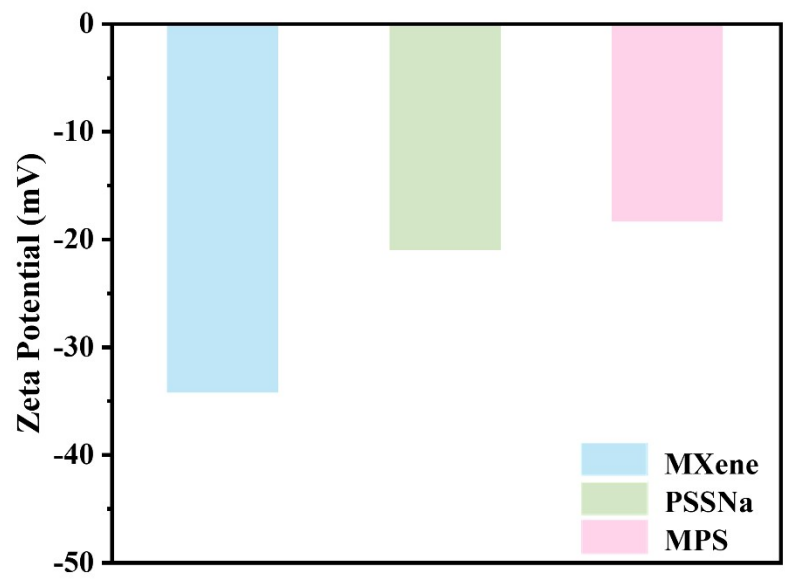


**Figure S5.** Zeta potential of MXene, PSSNa and MPS.

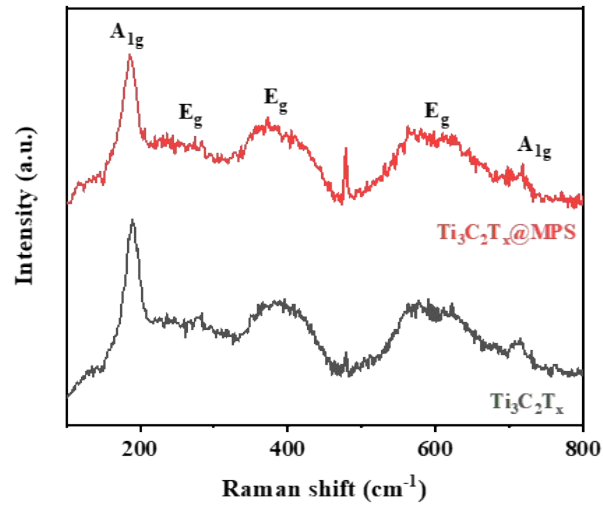


**Figure S6.** Raman spectra of Ti<sub>3</sub>C<sub>2</sub>T<sub>x</sub> and Ti<sub>3</sub>C<sub>2</sub>T<sub>x</sub>@MPS.

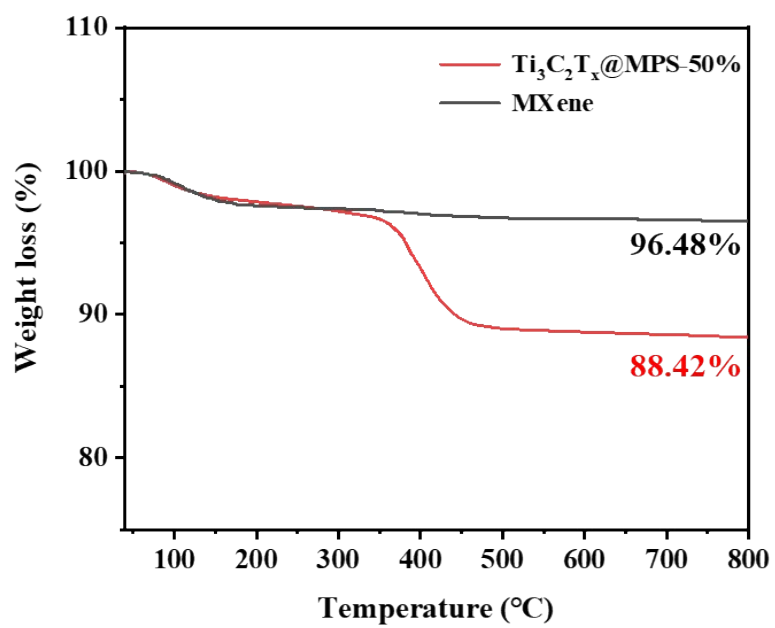


**Figure S7.** TGA curves of  $\text{Ti}_3\text{C}_2\text{T}_x$  and  $\text{Ti}_3\text{C}_2\text{T}_x@\text{MPS}$  films.

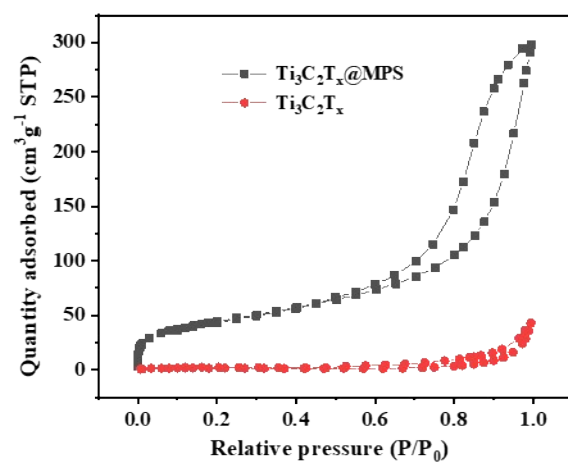


**Figure S8.** N<sub>2</sub> adsorption/desorption isotherms of pure Ti<sub>3</sub>C<sub>2</sub>T<sub>x</sub>@MPS film and MXene film.

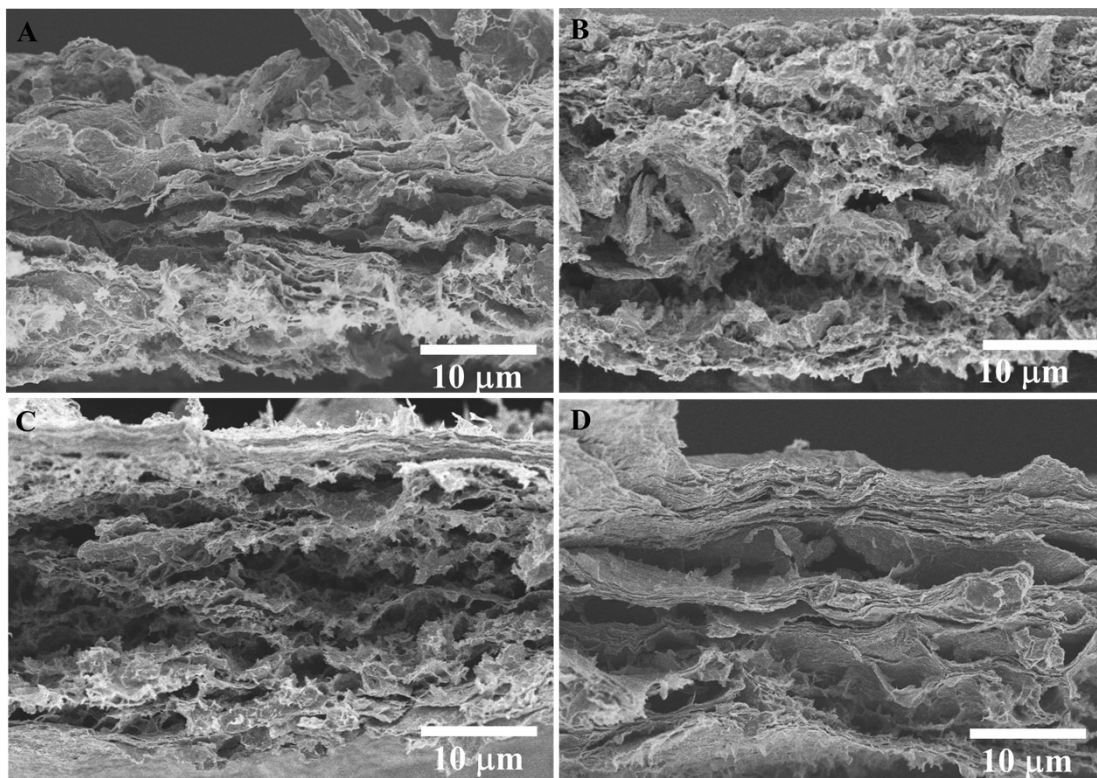


**Figure S9.** SEM of (A)  $\text{Ti}_3\text{C}_2\text{T}_x\text{@MPS-80\%}$ , (B)  $\text{Ti}_3\text{C}_2\text{T}_x\text{@MPS-70\%}$ , (C)  $\text{Ti}_3\text{C}_2\text{T}_x\text{@MPS-30\%}$ , (D)  $\text{Ti}_3\text{C}_2\text{T}_x\text{@MPS-20\%}$

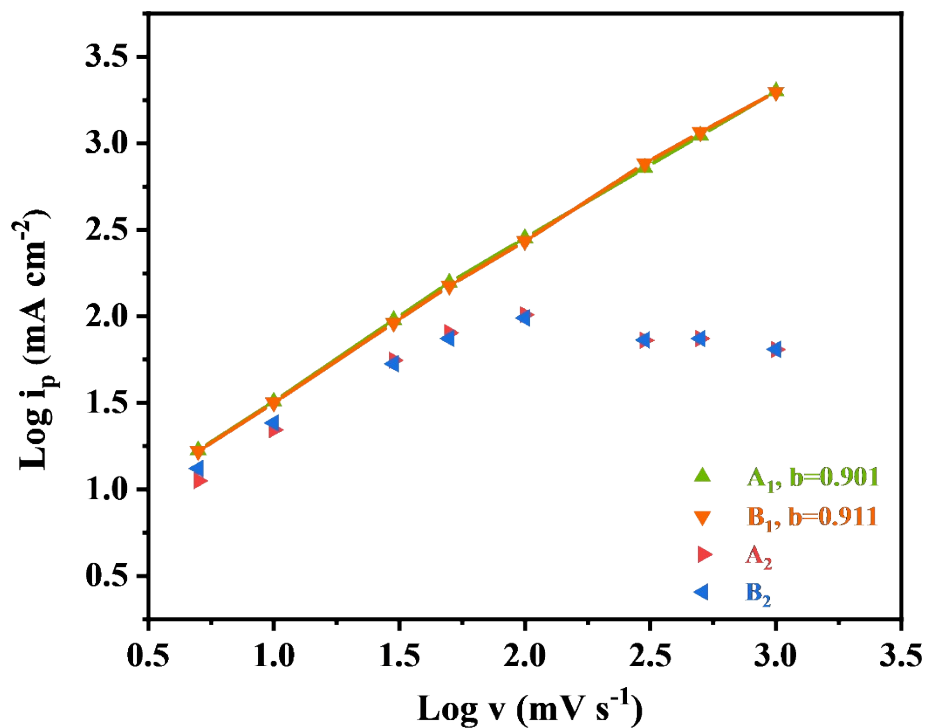


**Figure S10.** Plot of logarithm of anodic and cathodic peak current versus logarithm of scan rate for  $\text{Ti}_3\text{C}_2\text{T}_x@\text{MPS}$  film and pure MXene film. Theoretical analysis of electrochemical behaviors for  $\text{Ti}_3\text{C}_2\text{T}_x@\text{MPS}$  electrodes.

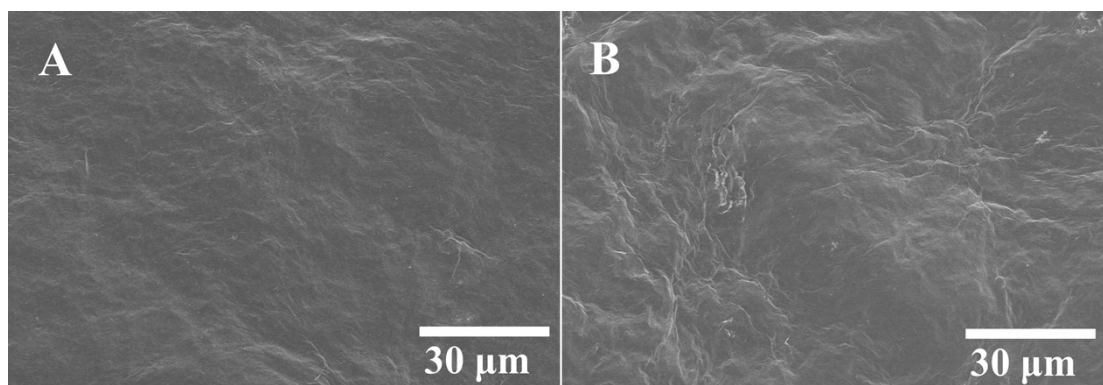


**Figure S11.** Top-view SEM images of the  $\text{Ti}_3\text{C}_2\text{T}_x@\text{MPS}$  electrode films (A) before and (B) after the cyclic tests for 10,000 cycles.

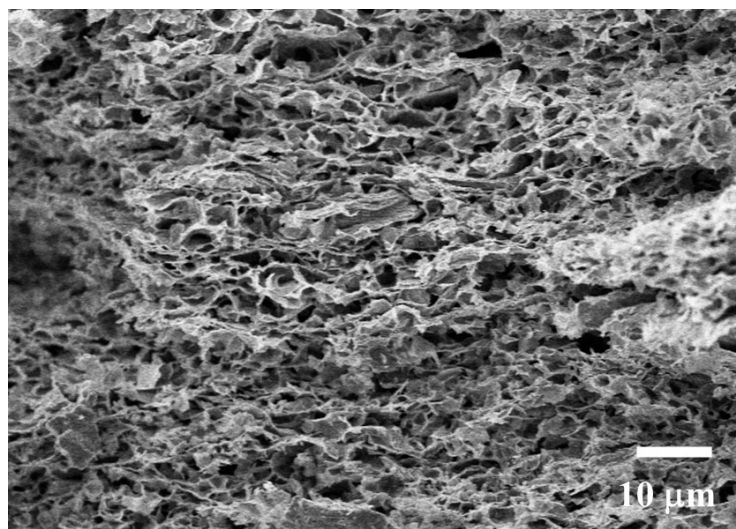


**Figure S12.** Cross-section SEM images of the Ti<sub>3</sub>C<sub>2</sub>T<sub>x</sub>@MPS electrode films after the cyclic tests for 10,000 cycles.

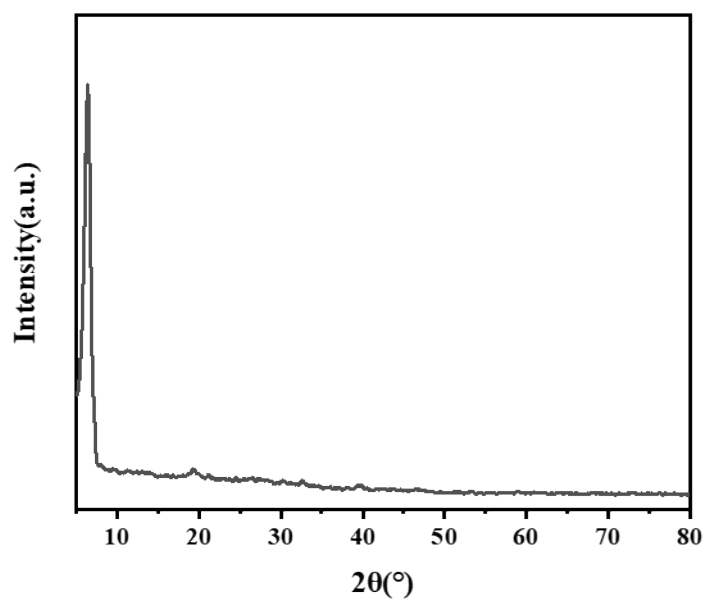


**Figure S13.** XRD spectroscopy of the  $\text{Ti}_3\text{C}_2\text{T}_x@\text{MPS}$  electrode films after the cyclic tests for 10,000 cycles.

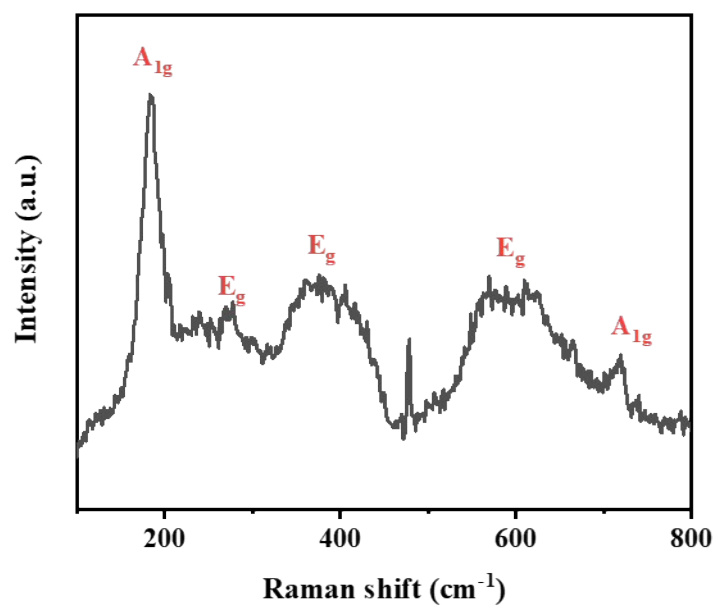


**Figure S14.** Raman spectroscopy of the Ti<sub>3</sub>C<sub>2</sub>T<sub>x</sub>@MPS electrode films after the cyclic tests for 10,000 cycles.

**Table S1. Comparison of electrochemical performance between MXene-based electrodes in aqueous supercapacitors.**

Materials	Electrolyte	Mass loading (mg cm <sup>-2</sup> )	Test condition	C <sub>g</sub> (F g <sup>-1</sup> )	Ref.
MXene/Graphdiyne nanotube composite films	1M H <sub>2</sub> SO <sub>4</sub>	-	5 mV s <sup>-1</sup>	314.4	[3]
Ti <sub>3</sub> C <sub>2</sub> T <sub>x</sub> @Chitosan films	3M H <sub>2</sub> SO <sub>4</sub>	4	5 mV s <sup>-1</sup>	425.8	[4]
MXene/carbon nanotube composite aerogel	3M H <sub>2</sub> SO <sub>4</sub>	-	0.3 A g <sup>-1</sup>	142.5	[5]
Ti <sub>3</sub> C <sub>2</sub> T <sub>x</sub> -Ni films	3 M H <sub>2</sub> SO <sub>4</sub>	1.2	2 mV s <sup>-1</sup>	369	[6]
MXene Hydrogel	3 M H <sub>2</sub> SO <sub>4</sub>	-	5 mV s <sup>-1</sup>	393	[7]
Carbon Dots-Intercalated MXene Film	3 M H <sub>2</sub> SO <sub>4</sub>	2.1	1 A g <sup>-1</sup>	344.9	[8]
MXene-hemicellulose films	1M H <sub>2</sub> SO <sub>4</sub>	-	10 mV s <sup>-1</sup>	366	[9]
I-PANI/MXene films	1M H <sub>2</sub> SO <sub>4</sub>	-	5 mV s <sup>-1</sup>	385	[10]
<b>Ti<sub>3</sub>C<sub>2</sub>T<sub>x</sub>@MPS</b>	<b>3 M H<sub>2</sub>SO<sub>4</sub></b>	<b>4</b>	<b>5 mV s<sup>-1</sup></b>	<b>469</b>	<b>This work</b>

**Table S2. EXAFS fitting parameters at the Ti K-edge for various samples ( $S_0^2=0.73$  from Ti-foil)**

	shell	CN <sup>a</sup>	R <sup>b</sup> (Å)	$\sigma^{2c}$ (Å <sup>2</sup> )	$\Delta E_0^d$ (eV)	R factor
Ti-foil	Ti-Ti	12	2.90±0.01	0.0079	5.0±0.6	0.0080
Sample	Ti-O/C	1.9±0.3	2.01±0.02	0.0024	-3.8±2.0	0.0176
	Ti-Ti	2.5±0.3	2.94±0.02	0.0019	-9.5±1.0	

<sup>a</sup>CN: coordinatin numbers; <sup>b</sup>R: bond distance; <sup>c</sup> $\sigma^2$ : Debye-Waller factors; <sup>d</sup>  $\Delta E_0$ : the inner potential correction. R factor: goodness of fit. Error bounds that characterize the structural parameters obtained by EXAFS spectroscopy were estimated as CN ± 20%; R ± 1%;  $\sigma^2$  ± 20%.

**Table S3. Comparison of electrochemical performance between MXene-based supercapacitors.**

Electrode materials	Configuration	Electrolyte	Voltage (V)	Capacitance (mF cm <sup>-2</sup> )	Max Energy density ( $\mu$ Wh cm <sup>-2</sup> )	Max Power density (mW cm <sup>-2</sup> )	Ref.
MoS <sub>2</sub> /Ti <sub>3</sub> C <sub>2</sub> T <sub>x</sub> //dMnO <sub>2</sub>	asymmetric	PVA/Na <sub>2</sub> SO <sub>4</sub>	1.8	153	68.8	27	[11]
MXene//RuO <sub>2</sub>	asymmetric	PVA/H <sub>2</sub> SO <sub>4</sub>	1.5	60	37	40	[12]
MXene/graphene	symmetric	PVA/Na <sub>2</sub> SO <sub>4</sub>	0.8	3.84	0.533	20	[13]
Ti <sub>3</sub> C <sub>2</sub> T <sub>x</sub> /CNT/PC	symmetric	PVA/KOH	1.2	212	10.5	2.19	[14]
MXene/BC	symmetric	Na <sub>2</sub> SO <sub>4</sub> /CMC	0.8	346	15	0.375	[15]
CNTs@MnO <sub>2</sub> //MXene/BC@PPy	asymmetric	MnSO <sub>4</sub> /PAM	1.9	290	145.4	3.78	[16]
Ti <sub>3</sub> C <sub>2</sub> T <sub>x</sub> -hBN-Ti <sub>3</sub> C <sub>2</sub> T <sub>x</sub>	symmetric	3 M H <sub>2</sub> SO <sub>4</sub>	0.6	200	24.1	209.2	[17]
Ti <sub>3</sub> C <sub>2</sub> T <sub>x</sub> @LDH-Ag//AC	asymmetric	PVA/KOH	1.6	-	22.31	33.028	[18]
Ti <sub>3</sub> C <sub>2</sub> -Cu	symmetric	H <sub>2</sub> SO <sub>4</sub>	1.6	290.5	103.3	8	[19]
PANI//Ti <sub>3</sub> C <sub>2</sub> T <sub>x</sub>	asymmetric	3 M H <sub>2</sub> SO <sub>4</sub>	1.4	925	252	34.02	[20]
CNTs@PPy//Ti <sub>3</sub> C <sub>2</sub> T <sub>x</sub>	asymmetric	PVA/H <sub>2</sub> SO <sub>4</sub>	1.4	150.22	40.49	0.26	[21]
<b>Ti<sub>3</sub>C<sub>2</sub>T<sub>x</sub>@MPS</b>	<b>symmetric</b>	<b>PVA/H<sub>2</sub>SO<sub>4</sub></b>	<b>0.8</b>	<b>905</b>	<b>80.04</b>	<b>180.4</b>	<b>This work</b>

## Note S1

### Calculations:

1. The mass specific capacitance ( $C_m$ , F g<sup>-1</sup>) of the electrode material can be calculated using GCD curve and CV curve, and the formulas are as follows

$$C_m = \frac{I\Delta t}{m\Delta V}$$

$$C_m = \frac{\int IdV}{mv\Delta V}$$

Where I (A) is the current,  $\Delta t$  (s) is the discharge time, m (g) is the mass of the active substance in the electrode material,  $\Delta V$  (V) is the potential window of the test, and v (V s<sup>-1</sup>) is the scanning rate.

2. The area capacitance ( $C_a$ , mF cm<sup>-2</sup>) of the material can be calculated using the CV curve as follows

$$C_a = \frac{\int IdV}{Sv\Delta V}$$

Where, I (mA) is the discharge current,  $\Delta V$  (V) is the potential window of the test, v (mV s<sup>-1</sup>) is the scanning rate, and  $\Delta V$  (V) is the potential window of CV.

3. The power density (P, W kg<sup>-1</sup>) and energy density (E, Wh kg<sup>-1</sup>) of the flexible symmetric supercapacitor are calculated by the following formula

$$E = \frac{(C \times \Delta V^2)}{2 \times 3.6}$$

$$P = \frac{E \times 3600}{\Delta t}$$

Where C (F g<sup>-1</sup>) is the specific capacitance of the device,  $\Delta V$  (V) is the potential window of the device, and  $\Delta t$  (s) is the discharge time of the device.

## References :

- [1] H. Funke, A.C. Scheinost, M. Chukalina, Wavelet analysis of extended x-ray absorption fine structure data, *Phys. Rev. B* 71(9) (2005) 7.
- [2] H. Funke, M. Chukalina, A.C. Scheinost, A new *FEFF*-based wavelet for EXAFS data analysis, *J. Synchrotr. Radiat.* 14 (2007) 426-432.
- [3] Y. Wang, N. Chen, Y. Liu, X. Zhou, B. Pu, Y. Qing, M. Zhang, X. Jiang, J. Huang, Q. Tang, B. Zhou, W. Yang, MXene/Graphdiyne nanotube composite films for Free-Standing and flexible Solid-State supercapacitor, *Chemical Engineering Journal* 450 (2022).
- [4] Y. Ding, Y. Liu, X. Sun, Y. Yao, B. Yuan, T. Huang, J. Tang, Three-dimensional ordered and porous Ti<sub>3</sub>C<sub>2</sub>T<sub>x</sub>@Chitosan film enabled by self-assembly strategy for high-rate pseudocapacitive energy storage, *Chemical Engineering Journal* 442 (2022).
- [5] T. Xu, Y. Wang, K. Liu, Q. Zhao, Q. Liang, M. Zhang, C. Si, Ultralight MXene/carbon nanotube composite aerogel for high-performance flexible supercapacitor, *Advanced Composites and Hybrid Materials* 6(3) (2023).
- [6] H. Xu, J. Fan, H. Su, C. Liu, G. Chen, Y. Dall'Agnesse, Y. Gao, Metal Ion-Induced Porous MXene for All-Solid-State Flexible Supercapacitors, *Nano Letters* 23(1) (2022) 283-290.
- [7] X. Huang, J. Huang, D. Yang, P. Wu, A Multi-Scale Structural Engineering Strategy for High-Performance MXene Hydrogel Supercapacitor Electrode, *Advanced Science* 8(18) (2021).
- [8] P. Zhang, J. Li, D. Yang, R.A. Soomro, B. Xu, Flexible Carbon Dots-Intercalated MXene Film Electrode with Outstanding Volumetric Performance for Supercapacitors, *Advanced Functional Materials* 33(1) (2022).
- [9] R. Chen, H. Tang, Y. Dai, W. Zong, W. Zhang, G. He, X. Wang, Robust Bioinspired MXene–Hemicellulose Composite Films with Excellent Electrical Conductivity for Multifunctional Electrode Applications, *ACS Nano* 16(11) (2022) 19124-19132.
- [10] J. Wang, D. Jiang, M. Zhang, Y. Sun, M. Jiang, Y. Du, J. Liu, Ice crystal-assisted intercalation of PANI within Ti<sub>3</sub>C<sub>2</sub>T<sub>x</sub> MXene thin films for flexible supercapacitor electrodes with simultaneously high mechanical strength and rate performance, *Journal of Materials Chemistry A* 11(3) (2023) 1419-1429.
- [11] F. Wan, X. Wang, C. Tang, C. Jiang, W. Wang, B. Li, Y. Zhang, X. Zhu, Metallic 1T-MoS<sub>2</sub> coupled with MXene towards ultra-high rate-capabilities for supercapacitors, *Journal of Materials Chemistry A* 10(22) (2022) 12258-12268.
- [12] Q. Jiang, N. Kurra, M. Alhabeab, Y. Gogotsi, H.N. Alshareef, All Pseudocapacitive MXene-RuO<sub>2</sub> Asymmetric Supercapacitors, *Advanced Energy Materials* 8(13) (2018).
- [13] D. Wen, G. Ying, L. Liu, Y. Li, C. Sun, C. Hu, Y. Zhao, Z. Ji, J. Zhang, X. Wang, Direct inkjet printing of flexible MXene/graphene composite films for supercapacitor electrodes, *Journal of Alloys and Compounds* 900 (2022).
- [14] K. Yang, M. Luo, D. Zhang, C. Liu, Z. Li, L. Wang, W. Chen, X. Zhou, Ti<sub>3</sub>C<sub>2</sub>T<sub>x</sub>/carbon nanotube/porous carbon film for flexible supercapacitor, *Chemical Engineering Journal* 427 (2022).
- [15] M. Weng, J. Zhou, Y. Ye, H. Qiu, P. Zhou, Z. Luo, Q. Guo, Self-chargeable supercapacitor made with MXene-bacterial cellulose nanofiber composite for wearable devices, *Journal of Colloid and Interface Science* 647 (2023) 277-286.
- [16] W. Cheng, J. Fu, H. Hu, D. Ho, Interlayer Structure Engineering of MXene-Based Capacitor-Type Electrode for Hybrid Micro-Supercapacitor toward Battery-Level Energy Density, *Advanced Science* 8(16) (2021).

- [17] W. Yang, J.J. Byun, J. Yang, F.P. Moissinac, Y. Ma, H. Ding, W. Sun, R.A.W. Dryfe, S. Barg, All-In-One MXene–Boron Nitride–MXene “OREO” with Vertically Aligned Channels for Flexible Structural Supercapacitor Design, *ACS Applied Energy Materials* 4(8) (2021) 7959-7972.
- [18] C. Zhang, R. Guo, H. Wang, X. Xie, C. Du, Composite electrodes with NiCoAl-LDH coated Ti<sub>3</sub>C<sub>2</sub>T<sub>x</sub> MXene and incorporated Ag nanowires for screen-printable in-plane hybrid supercapacitors on textiles, *Applied Surface Science* 598 (2022).
- [19] Y. Bai, C. Liu, T. Chen, W. Li, S. Zheng, Y. Pi, Y. Luo, H. Pang, MXene-Copper/Cobalt Hybrids via Lewis Acidic Molten Salts Etching for High Performance Symmetric Supercapacitors, *Angewandte Chemie International Edition* 60(48) (2021) 25318-25322.
- [20] Y. Wang, X. Wang, X. Li, Y. Bai, H. Xiao, Y. Liu, R. Liu, G. Yuan, Engineering 3D Ion Transport Channels for Flexible MXene Films with Superior Capacitive Performance, *Advanced Functional Materials* 29(14) (2019).
- [21] Z. Li, J. Song, H. Hu, C. Yuan, M. Wu, D. Ho, Rolled-up island-bridge (RIB): a new and general electrode configuration design for a wire-shaped stretchable micro-supercapacitor array, *Journal of Materials Chemistry A* 9(5) (2021) 2899-2911.